ATLAS Internal Note
PHYS-NO-XXX
22 Oct 1998

The Discovery Potential of a Heavy Higgs ($m_H \geq 800$ GeV) Using Full GEANT Simulation of the ATLAS Detector.

P. Savard[1] and G. Azuelos
Université de Montréal, Québec
Canada

Oct 22, 1998

[1]Now at University of Toronto, Ontario, Canada

Abstract

Full GEANT simulation of the process of heavy Higgs ($m_H \geq 800$ GeV) production by W gluon fusion (q q $\rightarrow$ q q H $\rightarrow$ q q W W $\rightarrow$ q q lν jj), as well as backgrounds $t\bar{t}$ and $W + jets$ have been performed. The efficiencies for reconstructiong the W $\rightarrow$ jet-jet decay, for vetoing jets in the central region ($|\eta < 2.0|$) and for tagging jets in the forward regions ($2.0 < |\eta| < 4.9$) have been evaluated, with particular attention given to high luminosity ($\mathcal{L} = 10^{34}$ cm^{-2}s^{-1}) pile-up noise. The discovery potential for a heavy Higgs is then evaluated. We confirm previous particle level results which concluded that 3 years running at low luminosity ($\mathcal{L} = 10^{33}$ cm^{-2}s^{-1}) would be sufficient to discover a heavy Higgs in the H $\rightarrow$ WW $\rightarrow l\nu jj$ channel.

1 Introduction

One of the main goals of the LHC and of the ATLAS detector is to better understand the mechanism underlying the breaking of electroweak symmetry. Today, in the framework of the Standard Model, precision electroweak measurements from LEP and SLC, together with the known mass of the top, lead to the indirect determination of a relatively low mass ($m_H < 220$ GeV, 90% C.L.) for the Higgs scalar [1]. However, systematic uncertainties can be quite large, since predictions vary widely when some measurements are excluded from the calculation [2]. Theoretically, the mass of a Standard Model Higgs is bounded by requirements of vacuum stability and validity of the running of the effecting coupling. In this model, as the Higgs mass increases, gauge boson coupling becomes stronger, eventually ($m_H \sim 1.6$ TeV) leading to violation of perturbative unitarity. However, the Standard model is known to suffer from gauge hierarchy problems: radiative corrections to the mass of the Higgs boson itself are divergent and positive, which make it unnatural to have a low scale for electroweak symmetry breaking [3]. For that reason, aside from adopting alternative theories such as supersymmetry, it is essential, in the absence of a low mass Higgs, to study W pair boson scattering at high mass. In this note, we consider as a reference case for such processes the search for a very heavy Higgs ($M_H \sim 800 - 1000$ GeV).

The most promising discovery channels in this mass range are H $\rightarrow$ WW $\rightarrow l\nu jj$, H $\rightarrow$ ZZ $\rightarrow lljj$. The observability in ATLAS of the process $H \rightarrow ZZ \rightarrow ll\nu\nu$, which is also very important, has been studied by [4]. For a study of the process H $\rightarrow$ WW $\rightarrow l\nu jj$ for Higgs masses below 600 GeV, see [5]. Previous studies [6, 7, 8] have indicated that a heavy Higgs could be found within 3 years at low luminosity running (3×10^4 pb^{-1}) with the H $\rightarrow$ WW $\rightarrow l\nu jj$ channel. These studies demonstrated the importance of jet vetoing, forward jet tagging and a good reconstruction of the W mass (W $\rightarrow$ jet jet) in reducing the main backgrounds ($t\bar{t}$ and W+jets). However, these studies relied on particle level simulations and the results are thus subject to potentially important uncertainties. The tagging of jets in the forward region for instance, requires the reconstruction of low p_T but high energy jets in a very compact area where calorimeter shower effects can be large. The H $\rightarrow$ ZZ $\rightarrow lljj$ channel is only briefly mentioned in this note and detailed studies can be found elsewhere [9, 10]. It cannot be considered as a discovery channel since more than 1 year at high luminosity (10^5 pb^{-1})

would be required to observe a signal (with a 5 σ significance).

In the first part of this note we evaluate, using a detailed GEANT simulation of the ATLAS detector, the efficiencies for reconstructing the W $\rightarrow$ jet-jet decay, the vetoing of jets in the central region ($|\eta|$ <2.0) and jet tagging in the forward region ($|\eta|$ >2.0). In the second part, we use those efficiencies to evaluate the discovery potential of a heavy Higgs.

In the following sections we first give an an overview of the signal and backgrounds. Then, the software used is these studies is described along with the methods used to generate pile-up events and to calibrate the jet energies. Efficiencies for W $\rightarrow$ jet-jet reconstruction and for central jet vetoing are evaluated. A section is devoted on the description of the methods used to reconstruct jets in the forward region of the calorimeter and to evaluate the forward jet tagging efficiency. Finally, the conclusions on the discovery potential for a heavy Higgs (800 GeV and 1 TeV) with the H $\rightarrow$ WW $\rightarrow$ $l\nu jj$ channel are given, and the precision with which one could reconstruct the mass, width and cross section of the scalar boson is evaluated.

2 The H $\rightarrow$ WW $\rightarrow$ $l\nu jj$ channel

A Feynman diagram of the H $\rightarrow$ WW $\rightarrow$ $l\nu jj$ channel is given in figure 1. The kinematics of the signal are characterized by:

- A high p_T lepton in the central region ($|\eta| < 2.0$).
- Missing transverse energy due to the escaping neutrino.
- Two high p_T jets in the central region from the decay of a W. Due to the W boost, the two jets are very close together (ΔR $\sim$0.4).
- A forward and backward jet around $|\eta| = 3.2$ for a 1 TeV Higgs.
- Apart from the two jets from the W, there is little hadronic activity in the central region.

The main backgrounds for the H $\rightarrow$ WW $\rightarrow$ $l\nu jj$ channel are $t\bar{t}$, W+jets ,WZ and WW. For the H $\rightarrow$ ZZ $\rightarrow$ $lljj$ channel , two leptons can

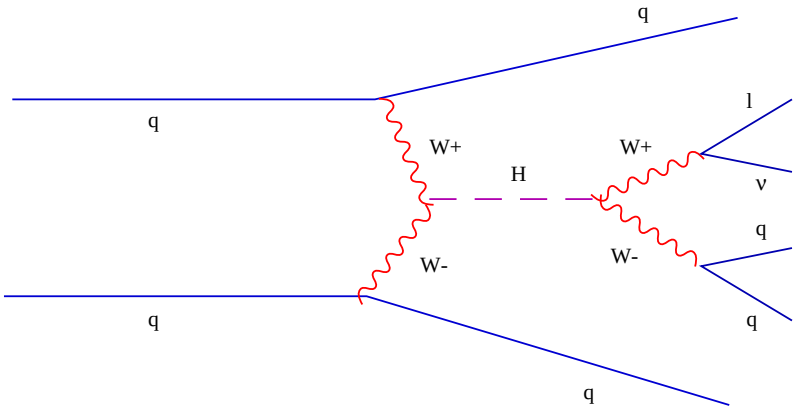

Figure 1: Feynman diagram of the H $\rightarrow$ WW $\rightarrow l\nu jj$ signal.

be reconstructed (as opposed to one lepton and missing E_T in the previous case) and a cut on the dilepton invariant mass can be applied. For this reason, the $t\bar{t}$ background is negligible and the main backgrounds are then Z+jets, WZ and ZZ. The cross sections for signal and backgrounds are given in table 2.

To extract the signal from the backgrounds we use the following strategies:

- The p_T spectrum of the Higgs decay products is much higher than that of the backgrounds. We therefore impose high p_T cuts on the lepton, missing E_T and on the jets coming from the W.
- Since there are two nearby jets to reconstruct, we require that two jets be reconstructed close together using a small ΔR=0.2 cone.
- A cut on the reconstructed invariant mass of the two jets will be used.
- In the case of the signal, only two jets should be reconstructed in the central region. A veto on extra jets is therefore imposed to reduce the $t\bar{t}$ background.
- Two jets will be searched for in the forward and backward ($|\eta| > 2.0$) regions of the detector.

Process	$\sigma \cdot Br$ (pb)	# events 3×10^4 pb^{-1}	# events 10^5 pb^{-1}
H $\rightarrow$ WW $\rightarrow l\nu jj$ $m_H = 1$ TeV (lepton: μ or e)	0.016	$\sim$ 500	$\sim$ 1500
$t\bar{t} \rightarrow WW \rightarrow l\nu jj$ +2 b jets p_T(top) $>$ 50 GeV	150	$4.5 \cdot 10^6$	$1.5 \cdot 10^7$
W + jets p_T (W) $>$ 50 GeV	1900	$6 \cdot 10^7$	$1.8 \cdot 10^8$
WW p_T (W) $>$ 50 GeV	8.5	250000	850000
H $\rightarrow$ ZZ $\rightarrow lljj$ (leptons: μ or e)	0.003	$\sim$80	$\sim$270
Z + jets p_T (Z) $>$ 50 GeV	255	$7.7 \cdot 10^6$	$2.5 \cdot 10^7$
ZZ p_T (Z) $>$ 50 GeV	.5	15000	50000

Table 1: Cross section for the signal and backgrounds.

To compare to results obtained in [8], we will use the following cuts in the central region, given in table 2 for H $\rightarrow$ WW $\rightarrow l\nu jj$ and H $\rightarrow$ ZZ $\rightarrow$ $lljj$ signals. These cuts will be referred to as the "high p_T" cuts.

Also for the purpose of comparison with past results, and for reasons which will be discussed in the second part of this note, we will use a second set of cuts which will be referred to as "loose p_T" cuts. These cuts are given in table 14.

3 Simulation and reconstruction Software

To evaluate the discovery potential of the signals described above, very large background event samples were generated. The Monte Carlo event generator used in this study was PYTHIA 5.7[11]. These samples were then simulated

Signal	H $\rightarrow$ WW $\rightarrow l\nu jj$
Lepton cuts	p_T^l, $p_T^\nu > 100$ GeV $p_T^{W\rightarrow l\nu} > 350$ GeV
Jet cuts	$p_T^{W\rightarrow jj} > 350$ GeV 2 jets de $p_T^j > 50$ GeV with ΔR=0.2
Mass cut	$m_W \pm 15$ GeV
Signal	H $\rightarrow$ ZZ $\rightarrow lljj$
Lepton cuts	$p_T^l > 100$ GeV $p_T^{Z\rightarrow ll} > 300$ GeV
Jet cuts	$p_T^{Z\rightarrow jj} > 300$ GeV 2 jets of $p_T^j > 50$ GeV with ΔR=0.2
Mass cut Z $\rightarrow$ l l	$m_Z \pm 8$ GeV
Mass cut Z $\rightarrow$ j j	$m_Z \pm 15$ GeV

Table 2: High p_T cuts for H $\rightarrow$ WW $\rightarrow l\nu jj$ and H $\rightarrow$ ZZ $\rightarrow lljj$.

with the ATLFAST 1.0[12] parameterized detector response package. For the efficiency studies presented in this note, smaller samples of fully simulated signal and background events were produced and compared to ATLFAST. In the second part of this note, corrections based on these comparisons are applied to the larger event samples of ATLFAST.

The detailed simulation of the detector response was done using GEANT 3.21[13]. Two separate geometric descriptions were used: DICE and a standalone program for the forward calorimeter (described later). The version of DICE used was 95-6 and the hadronic shower package was GEANT-FLUKA. Although the geometry of the detector has undergone some important changes since that version, the differences between the results that follow and the ones that would be obtained with the very latest geometry are expected to be minor. This assertion is justified by the fact that jets are less sensitive to small scale geometric features and that few of the jets in the samples quoted above are in the barrel-endcap transition region.

Cuts	H $\rightarrow$ WW $\rightarrow l\nu jj$	H $\rightarrow$ ZZ $\rightarrow lljj$
Lepton cuts	$p_T^l,\ p_T^\nu > 50$ GeV $p_T^{W\rightarrow l\nu} > 150$ GeV	$p_T^{l_1},\ p_T^{l_2} > 50$ GeV $p_T^{Z\rightarrow ll} > 150$ GeV
Jet cuts	$p_T^{W\rightarrow jj} > 150$ GeV 2 jets de $p_T^j > 50$ GeV avec ΔR=0.2	$p_T^{Z\rightarrow jj} > 150$ GeV idem
Mass cut	$m_W \pm 10$ GeV	$m_Z \pm 15$ GeV

Table 3: Loose p_T cuts for H $\rightarrow$ WW $\rightarrow l\nu jj$.

To generate high luminosity (10^{34} cm^{-2}s^{-1}) pile-up noise, minimum bias events were simulated using DICE. The details of this procedure are given in [14] of which a short summary is given here. To build the pile-up "event", a random number of events per bunch crossing was chosen using a Poisson distribution with a mean of 23. Then, the energy response of each bunch crossing was convoluted with the shaping functions of the various calorimeters. The barrel and endcap liquid Argon calorimeters use bipolar shaping whose response to a triangular input pulse lasts for over 500 ns. This means that the energy deposition of over 20 bunch crossings must be considered. In the case of the Tile calorimeter, a gaussian with FWHM of 50 nanoseconds was used as the shaping response. To reduce the effect of pile-up noise, a 1 GeV E_T cell level cut was applied to each 0.1 x 0.1 ($\Delta\eta \times \Delta\phi$) calorimeter tower. For more details on the method used and the properties of pile-up noise in the calorimetry system, see [14, 15, 16]

For the simulations which used DICE, the program used to reconstruct the events was ATRECON (95-6). The jets used here, reconstructed at calorimeter level with the standard fixed cone jet finder, were considered massless. The algorithm that was used to find jets was the standard fixed cone jet finder provided in this version of ATRECON. A cone of ΔR=0.4 was chosen to limit the effect of minimum bias pile-up noise.

The standard energy calibration of ATRECON was applied, with some changes based on more recent Monte Carlo results [15]. On top of that, the jet energy scale had to be adjusted on a case by case basis depending on the cone size used and whether pile-up was included. The jet energy scale was

set by multiplying the reconstructed jet energy by the average of the ratio of the parton energies to the reconstructed jet energies. This needed to be done for every reconstruction method, cone size and cell E_T cut used (when pile-up is added).

4 W $\rightarrow$ jet-jet

A detailed study of the reconstruction of the W $\rightarrow$ jet-jet decay and its associated systematic effects over a wide range of transverse energies can be found in [18]. We give here a summary of the reconstruction methods used for overlapping, high-p_T W.

4.1 Algorithms

Three methods were used to determine the invariant mass of the W:

- Method 1
  - The mass was simply calculated from the 4-momenta of each jet (the cone size is ΔR=0.4):

$$M_W{}^2 = (P^{\mu}{}_{(j1)} + P^{\mu}{}_{(j2)})(P_{\mu_{(j1)}} + P_{\mu_{(j2)}})$$

- Method 2
  - The mass was calculated by taking into account the "4-momentum" of each calorimeter cell included in the two ΔR=0.4 jet cones. The baricenter of each jet was found using ΔR=0.2 cones.

$$M_W{}^2 = (\sum_{i=1}^{N_{cells}} P^{\mu}_{cell_i})^2$$

- Method 3
  - Same technique as the second method but the energy was collected in only one cone of ΔR =0.5 or 0.6. This last method is used only when the two jets from the decay of a high p_T W severely overlap.

The advantage of the third method is that it is not necessary to employ an energy sharing scheme when the two jets overlap. For method 2, energy sharing is only needed to determine the jet baricenters. This defines the list of cells that will be used in the mass reconstruction. Once the cell list is determined, no energy sharing is required and the evaluation of the angle between the two jets is not needed since the known angle of each cell is used. In the case of method 1 however, the energy of each jet has to be determined as well as the angle between them. To do this, the centroid of each jet was obtained by sharing the energies according to the following steps:

- In the first iteration, all the energy in the overlap was assigned to one jet and the jet momenta were calculated.
- In the second iteration, the energy in the overlap region was shared equally and the jet momenta were recalculated.
- Finally, the energy in the overlap region was shared in proportion to the jet energies calculated in the second step. The jet momenta were then calculated for the last time. In the case of the severely overlapping jets of the Higgs signal, another method was attempted for the sharing of energy: using the centroids obtained with the preceding steps, the energy of each jet was recalculated by assigning the energies of cells in the overlap region to the closest jet. This method provided a better reconstruction in the case when the two W are very close to each other.

It was shown in [18] that, due to transverse shower spreading, the reconstructed invariant mass using methods 2 and 3 suffered from a dependence on the p_T fo the W. This dependence can be cured by applying a linear correction as shown in figure 2. For method 2, the correction is about 4% for p_T W of 300 GeV and 15% for p_t W of 600 GeV.

4.2 Results for W $\rightarrow$ jet-jet reconstruction

Table 4 shows the signal W$\rightarrow$ jet-jet reconstruction efficiencies obtained with the various methods described above compared to results from ATLFAST and Zmushko et al [8]. As shown in the table, the efficiency results also take into account the lepton and jet cut efficiencies. There is a good agreement between the results obtained with full simulation (with and without pile-up),

Cuts	Zmushko et al.	ATLFAST with modif.	Full Sim. No pile-up	Full Sim. pile-up
# Events	5000	5000	4000	4000
Lepton cuts	42.5%	43.3%	42.6%	42.6%
Jet cuts	N/A	29.0%	29.8%	29.8%
Method 1	N/A	22.8%	21.0%	21.0%
Method 2	N/A	25.2%	24.8%	24.4%
Method 3 (.5)	23.6%	25.8%	24.8%	25.0%
Method 3 (.6)	N/A	26.1%	25.6%	25.1%
Central cuts				
No pile-up	N/A	25.2± .7%	24.8± .8%	-
with pile-up	23.6± .7%	N/A	-	24.4± .7%

Table 4: Efficiencies for the signal with high p_T central cuts compared to ATLFAST and Zmushko et al.

Zmushko et al [8]. and ATLFAST. Since all the reconstructed objects have very high p_T, pile-up noise has little influence on the recontruction efficiencies. This is not the case for W with lower p_T.

Table 5 shows the W→jet-jet reconstruction efficiencies for the signal and backgrounds using ATLFAST. The results are shown for a Higgs mass of 1 TeV. For lower Higgs masses, the p_T of the W is on average lower and the jet-jet separation is greater. Since method 2 is more flexible and can more easily handle variable jet-jet separations, it has been retained for the rest of the analysis.

Table 6 compares the W→jet-jet reconstruction efficiencies for the signal and backgrounds using full simulation of the detector. The set of "loose p_T" cuts (see table 14) were used. There is in general a very good agreement between the fast Monte Carlo and the full simulation. There is some discrepancy for $t\bar{t}$ and the efficencies for ATLFAST will be corrected accordingly in the note containing the final results.

# Events	Higgs 5000	$t\bar{t}$ $p_T > 300$ GeV 50000	W+jets $p_T > 250$ GeV 50000
Lepton cuts	43.3%	6.2%	11.5%
Jet cuts	29.0%	3.3%	2.3%
Method 1	22.8%	1.0%	.4%
Method 2*	25.2± .7%	1.00± .04%	.52± .03%
Method 3 (.5)	25.8%	1.2%	.68%
Method 3 (.6)	26.1%	.93%	.67%

Table 5: Reconstruction efficiencies for the signal and backgrounds using ATLFAST with high p_T cuts. The asterisk (*) denotes the method which has been retained for the analysis.

Table 7 shows a comparison of the W→ jet jet reconstruction efficiencies with and without high luminosity pile-up noise. Again, because of the very high p_T of the reconstructed objects, the effect of pile-up is minor.

4.3 Jet Profile and Energy Asymmetry

To reduce the main background (W+jets) further, other cuts can be considered besides the cut on the W invariant mass. Since the W is a color singlet object, the jets emitted in the decay should be more "pencil-like" than the gluon jets present in W+jets[2]. The idea of using jet profile to discriminate between signal and background was first described in [19]. In this analysis, the most sensitive variable found for the case without pile-up was the energy in annula around the two W jet candidates whose inner radii are 0.4 in $\eta - \phi$, and whose outer radii are 0.5. In the case with pile-up the radii were 0.3 and 0.4, respectively. The results are shown in figure 3. Without pile-up, a cut at 0.18 on the variable$(E_{cone5} - E_{cone4})/E_{cone5}$ removes 55% of the background while keeping 88% of the signal. With pile-up, a cut at 0.18

[2]The W in the W+jets background decays leptonically and two jets in the event need to have an invariant mass close to the W mass.

Process	DICE	ATLFAST
Higgs $M_W \pm$ 15 GeV	84.5 $\pm$ 1.9 GeV	84.3 $\pm$ 1.7 GeV
Higgs $M_W \pm$ 10 GeV	75.3 $\pm$ 1.8 GeV	74.2 $\pm$ 1.6 GeV
$t\bar{t}$ $M_W \pm$ 15 GeV	47.6 $\pm$ 2.8 GeV	42.5 $\pm$ 1.3 GeV
$t\bar{t}$ $M_W \pm$ 10 GeV	36.3 $\pm$ 2.5 GeV	33.9 $\pm$ 1.2 GeV
W+jets $M_W \pm$ 15 GeV	19.8 $\pm$ 1.4 GeV	21.6 $\pm$ 2.0 GeV
W+jets $M_W \pm$ 10 GeV	13.1 $\pm$ 1.1 GeV	14.4 $\pm$ 1.7 GeV

Table 6: Comparison of the W$\rightarrow$ jet-jet reconstruction efficiencies between DICE and ATLFAST. The generation cuts for the backgrounds are given in the text and the p_T cuts are described in section 2.

Process	Without pile-up	With Pile-up
Higgs $M_W \pm$ 15 GeV	84.5 $\pm$ 1.9 GeV	82.4 $\pm$ 1.9 GeV
Higgs $M_W \pm$ 10 GeV	75.3 $\pm$ 1.8 GeV	71.1 $\pm$ 1.7 GeV
$t\bar{t}$ $M_W \pm$ 15 GeV	47.6 $\pm$ 2.8 GeV	47.2 $\pm$ 2.8 GeV
$t\bar{t}$ $M_W \pm$ 10 GeV	36.3 $\pm$ 2.5 GeV	35.9 $\pm$ 2.4 GeV
W+jets $M_W \pm$ 15 GeV	19.8 $\pm$ 1.4 GeV	18.1 $\pm$ 1.4 GeV
W+jets $M_W \pm$ 10 GeV	13.1 $\pm$ 1.1 GeV	12.4 $\pm$ 1.2 GeV

Table 7: Comparison of the W$\rightarrow$ jet-jet reconstruction efficiencies with and without high luminosity pile-up noise.

on the $(E_{cone4} - E_{cone3})/E_{cone4}$ variable removes 50% of the background while keeping 85% of the signal.

Although this cut seems promising, even with the addition of pile-up noise, it is not used in the final analysis.

Another interesting feature of the signal is that the W bosons from the signal have longitudinal polarization. Therefore the jets from the W decay should have energies that are close to each other as opposed to the case of transverse polarization where the jets would have more asymmetric energies.

Although the W from $t\bar{t}$ is expected to be 70% longitudinally polarized for a top mass of 175 GeV, the jets from the W+jets background will likely have asymmetric energies. The jet energy asymmetry of the signal and backgrounds is shown in figure 4. The application of our analysis cuts, however, biases the distributions and renders this additional cut ineffective.

5 Jet Veto Efficiency

As mentioned in section 2, the relatively low jet activity in the central region for the signal can be used to reject the backgrounds, specifically $t\bar{t}$ which has two extra jets.

A comparison of the jet veto efficiency between ATLFAST and DICE is given in figure 5 as a function of the jet p_T threshold. The jet energy scale used is optimized for low p_t jets (25 GeV). ATLFAST gives efficiencies that are $\sim$5% higher for the signal.

The jet veto efficiency is given in figure 6 for the case with pile-up and compared to the previous case without pile-up. In the analysis a cut of 15 GeV on the jet p_T is used for the case without pile-up and 25 GeV for the case with pile-up.

In table 8, the jet veto efficiencies are compared to ATLFAST and results from Zmushko et al. The energy scale had to be adjusted when high luminosity pile-up is added. The numbers in parentheses represent the actual jet energy cut when the energy scale is properly taken into account. The discrepancy between the results in this note and previous results by Zmushko et al. are due to a different treatment of pile-up and of the evaluation of the jet energy scale.

6 Forward Jet Tagging Efficiency

At the time this analysis was done, the description of the forward calorimeter in DICE was inadequate. The forward jet tagging study had therefore to be

Cuts	Zmushko et al.	ATLFAST with modif.	Full Sim.
Without Pile-up 20 GeV (22.0 GeV)	70.4± .5%	70.7± .6%	66.9± .6%
Pile-up 20 GeV (18.8 GeV)	34.1± .4%	N/A	54.3± .6%
Without Pile-up 25 GeV (27.5 GeV)	N/A	N/A	69.5± .7%
Pile-up 25 GeV (25.0 GeV)	N/A	N/A	62.3± .7%
Without Pile-up 30 GeV (33.0 GeV)	74.4± .6%	74.6± .6%	71.2± .7%
Pile-up 30 GeV (31.25) GeV	54.9± .5%	N/A	66.8± .6%

Table 8: Jet veto efficiencies compared to ATLFAST and Zmushko et al. The numbers in parentheses are the actual p_T cuts once the energy scale is taken into account.

realized in two steps. For the jets going into the endcap calorimeter, the software used here was the same as in the other studies presented in this note. For the jets going into the forward calorimeter and the transition region between the endcap region and the forward region, a standalone GEANT simulation was used[3]. The geometry description of this standalone program featured a very detailed forward calorimeter with the "tile" readout structure shown in figure 7. It also had a description of the material in front of the calorimeter and around the beampipe.

The forward calorimeter readout cells do not have a projective geometry in η and ϕ, but are rather organized in x and y (orthogonal coordinates perpendicular to the proton beams). There are essentially two tile sizes in two regions: one going from η ~3.2 to η ~ 4.2 and the other from η ~4.2 to the acceptance limit at η ~4.9. It is therefore not possible to apply a fixed E_T cut on calorimeter towers since the tile sizes change continously in pseudorapidity space. It is important to note that even if the towers were projective, the use of fixed E_T cuts would not be optimal. This is due to the fact that in the very forward regions, the lateral spread of the showers becomes very significant and that this spreading occurs in Cartesian (x-y) space.

For the forward calorimeter, cuts based on the significance in cells, and

[3]The program was written by Peter Loch.

towers have been used. The significance is defined here as the the signal collected in a cell divided by the average pile-up noise energy rms.

In the region between η=2.0 and η=2.9 covered by DICE, the jets were reconstructed in the following way:

- Each 0.1×0.1 tower (in $\Delta\eta \times \Delta\phi$) above a 3 GeV E_T threshold is considered as potential jet seed. This threshold is 6 GeV when pile-up noise is included.

- The energy of each tower within a radius of ΔR=0.4 is added to the energy of the jet candidate. An E_T threshold of 1.5 GeV is imposed on the energy in the towers when pile-up is included.

- The energy of the jet is calibrated without pile-up noise using the known value of the quark energy. Then, the jet energy scale is adjusted to take into account the effect of the cuts and pile-up noise. Finally, a jet has to have a minimum corrected energy of 15 GeV to be considered "tagged".

In the region $2.9 < \eta < 4.9$, the standalone GEANT program is used. The energy deposited in each forward calorimeter tube is grouped in tiles. In the endcap region, we proceed as explained above. For the forward calorimeter, the pile-up energy rms is calculated for each tile of each longitudinal segment of the forward calorimeter. The jet reconstruction proceeds as follows:

- Tiles having a significance higher than 4 are considered as potential jet seeds. This cut can go as high as 10 when high luminosity pile-up noise is added.

- The energy in a tile is added to the candidate jet energy if its signficance is greater than 1.0 and it is within a radius of ΔR=0.4 of the seed cell.

- With pile-up noise, a cut is imposed on the significance in a ΔR=0.2 cone around the seed cell. This cut proved to be the most efficient discriminator between pile-up jets and signal jets.

- Finally, after calibration and the adjustment of the energy scale which depends on the cuts used, a corrected transverse energy of 15 GeV is required for the jet to be tagged.

Figure 8 shows the signal significance with and without pile-up noise. The top left plot shows the significance of the jet seed cell. The top right plot gives the total significance in a ΔR=0.2 cone (the sum is linear) around the seed sell. A cone of ΔR=0.4 is used in the bottom left plot. The transverse energy of the jet is shown in the bottom right plot.

6.1 Results for forward jet tagging

The top plot of figure 9 gives the average transverse energy of forward quarks as a function of η, for a Higgs mass of 1 TeV. It is important to note that the average p_T decreases as a function of η and that the tagging efficiency is not a function of the calorimeter acceptance alone but also depends on the kinematics of the physical process considered. Therefore, these efficiency plots should not be used for other physical processes[4]. The bottom plot gives a comparison of the jet tagging efficiency without pile-up between GEANT simulations and ATLFAST. The ATLFAST results show good agreement with the full Monte Carlo up to η=4.0. Beyond this value, the transverse shower development leads to out of cone (or calorimeter) energy losses in the full simulation.

The top half of figure 10 shows the reconstruction efficiencies obtained with the nominal cuts at high luminosity for different jet p_T thresholds. The number of fake jets, given on figure 10, decreases very rapidly with rising p_T thresholds. The bottom plot shows the optimized jet tagging efficiency for a fake tag rate of 10% for one whole hemisphere in the forward region ($2.0< \eta <4.9$). The optimization was done using the various significance cuts described earlier.

As will be shown in the next part of this note, the imposition of an energy cut on the tagged jets (in addition to an E_T cut) greatly helps in reducing backgrounds. For the backgrounds, the number of jets drops rapidly as a function of η. This is not the case for the signal where the average quark η is $\sim$3.2 for a 1 TeV Higgs. For a given p_T cut, an energy cut effectively selects higher rapidity jets. With a energy cut of 300 GeV the fake tag rate drops

[4] with the possible exception of single top, W-gluon production.

from 10% to 3%. The fake tag rate for a 600 GeV energy cut is not available due to insufficient statistics but should be well below 1%.

7 Results for H $\rightarrow$ WW $\rightarrow l\nu jj$

The heavy Higgs discovery potential using the H $\rightarrow$ WW $\rightarrow l\nu jj$ signal is evaluated in this section for integrated luminosities corresponding to three years at low luminosity (3×10^4 pb^{-1}) and for one year at high luminosity (10^5 pb^{-1}). We will neglect low-luminosity pile-up noise as the average number of minimum bias events per bunch crossing is expected to be around two.

A comparison of the results obtained with ATLFAST and a previous note by Zmushko et al. [6] will be given. Then, using the results of the efficiency studies described in earlier sections of this note, the ATLFAST reconstruction efficiencies for jet vetoing, forward jet tagging and the W$\rightarrow$ jet-jet reconstruction will be corrected to provide a better evaluation of the heavy Higgs discovery potential.

Table 9 gives the efficiencies of various cuts applied sequentially. In this table, "$p_T >$" is a cut at generator level on the allowed p_T values for hard 2 $\rightarrow$ 2 processes, defined in the rest frame of the hard interaction [5]. The results, obtained with ATLFAST using the reconstruction algorithms described earlier are compared to Zmushko et al[6].

Significance $S/\sqrt{B}$ and signal to noise ratios obtained with the "high" p_T cuts for a Higgs mass of 1 TeV, after 3 years at low luminosity are given in table 10. Table 11 gives the equivalent results for a Higgs mass of 800 GeV. The results were obtained with ATLFAST.

The significance and signal to background ratios are given in table 12 for Higgs masses of 1 TeV and 800 GeV. In this case full simulation reconstruction efficiencies obtained earlier are used to correct the ATLFAST efficiencies. The energy cut used for the forward jets is 300 GeV. Since the uncertainties on the background cross sections are large[6] we also show in this table the significance and signal to background ratios when the amount of background is doubled or tripled.

[5] This is the CKIN(3) parameter in PYTHIA.

[6] we estimate about 60% on the W+jets cross section [20] and we conservatively assume 50% on $t\bar{t}$.

	Higgs	$t\bar{t}$	W+jets	WW
		p_T >300 GeV	p_T >250 GeV	p_T >50 GeV
# Events	5000	800000	1600000	255000
Central cuts "high p_T" with mass cut	25.2%	1.0%	.56%	.25%
# Events (Method 2)	1266	7995	8993	612
Veto Eff.				
Veto 20 GeV	70.7%	5.3%	41.0%	54.1%
Veto 30 GeV	74.6%	10.2%	49.5%	63.6%
# Events Veto 20 GeV	895	427	3687	331
Tagging Efficiency				
2 Jets $E > 100$ GeV	66.0%	7.0%	2.5%	1.2%
# Events	591	30	93	4
2 Jets $E > 600$ GeV	25.4%	$< .5\%$	$<.5\%$	$<.5\%$
# Events	227	2	10	0

Table 9: Efficiencies of various cuts for the signal (M_H=1 TeV) and the main backgounds at low luminosity.

# of generated events 3 years low lumi.	Higgs M_H= 1 TeV 5000 486	$t\bar{t}$ $p_T >$ 300 GeV 800000 192000	W+jets $p_T >$ 250 GeV 1600000 448000	WW $p_T >$ 50 GeV 255000 255000	$\frac{S}{\sqrt{B}}$	$\frac{S}{B}$
Central cuts and W mass cut	123	1919	2518	612	1.7	.02
Veto 20 GeV	87	102	1032	331	2.3	.06
E jets$>$ 100 GeV	57	7.2	26	4	9.3	1.5
E jets$>$ 300 GeV	42	3.1	9.5	1	11.4	3.1
E jets$>$ 600 GeV	22	.5	2.8	0	12.1	6.7

Table 10: Number of events after three years at low luminosity running, for the signal and backgrounds, after the cuts shown. The results were obtained with ATLFAST using the "high" p_T cuts for a Higgs 1 TeV.

The corrected ATLFAST results for 1 year at high luminosity (with pile-up) are given in table 13. The fake tag rate is about 3% for one whole hemisphere. This translates to about 50% of background events being due to fake tags. This includes not only events with double fake tags but also one single fake tag and one "true" tag from the background event. These numbers were obtained with the nominal cut 300 GeV for the jet tag energy. The number of fake tags for an energy threshold of 600 GeV is not available due to lack of statistics but it is unlikely to be above 0.5%, for one hemisphere.

Finally, the reconstructed mass spectrum of the signal and backgrounds is given in Figure 11 for a cut of 100 GeV on the tagged jet energy. To reconstruct the Higgs mass, the longitudinal component of the neutrino momentum is required. It is obtained by constraining the $m_{l\nu}$ mass to the generated W mass. This gives in general two solutions for the longitudinal momentum of the neutrino. The solution was chosen in an arbitrary manner. It was verified that the reconstructed Higgs mass did not depend on the chosen solution.

	Higgs M_H= 800 GeV	$t\bar{t}$ $p_T >$ 300 GeV	W+jets $p_T >$ 250 GeV	WW $p_T >$ 50 GeV	$\frac{S}{\sqrt{B}}$	$\frac{S}{B}$
# of generated events	5000	800000	1600000	255000		
3 years low lumi.	1000	192000	448000	255000		
Central cuts with W mass cut	141	1919	2518	612	2.0	.03
Veto 20 GeV	95	102	1032	331	2.5	.06
E jets$>$ 100 GeV	66	7.2	26	4	10.8	1.8
E jets$>$ 300 GeV	48	3.1	9.5	1	13.0	3.5
E jets$>$ 600 GeV	23.6	.5	2.8	0	13.0	7.2

Table 11: Number of events after three years at low luminosity, for the signal and backgrounds. The results were obtained with ATLFAST using the "high" p_T cuts for a Higgs 800 TeV.

	Higgs	$t\bar{t}$ $p_T >$ 300 GeV	W+jets $p_T >$ 250 GeV	WW $p_T >$ 50 GeV	$\frac{S}{\sqrt{B}}$	$\frac{S}{B}$
# of generated events	5000	800000	1600000	255000		
3 years low lumi.	486/1000	192000	448000	255000		
M_H = 1 TeV	37.9	3.3	9.2	1.0	10.3	2.8
Double background	37.9	6.6	18.4	2.0	7.3	1.4
Triple background	37.9	9.9	27.6	3.0	6.0	0.9
M_H = 800 GeV	43.5	3.3	9.2	1.0	11.8	3.2
Double background	43.5	6.6	18.4	2.0	8.4	1.6
Triple background	43.5	9.9	27.6	3.0	6.8	1.1

Table 12: Number of events for the signal and backgrounds after three years at low luminosity. The results were obtained by taking into account full simulation reconstruction efficiencies. A cut of E $>$ 300 GeV was imposed on the forward jets. Also shown are the results when the background is doubled or tripled.

	Higgs	$t\bar{t}$ $p_T >$ 300 GeV	W+jets $p_T >$ 250 GeV	WW $p_T >$ 50 GeV	$\frac{S}{\sqrt{B}}$	$\frac{S}{B}$
# of generated events	5000	800000	1600000	255000		
1 year high lumi.	1618/3333	640000	1500000	855000		
M_H = 1 TeV	115	22	63	12.5	11.6	1.2
Double background	115	44	126	25	8.2	0.6
M_H = 800 GeV	130	22	63	12.5	13.2	1.3
Double background	130	44	126	25	9.3	0.7

Table 13: Number of events for the signal and background after one year at high luminosity. The results were obtained using the "high" p_T cuts. The ATLFAST results were corrected using the full simulation efficiencies and a cut of E > 300 GeV was imposed on the forward jets.

7.1 Discussion of H $\rightarrow$ WW $\rightarrow l\nu jj$ results

For a Higgs mass of 1 TeV, a significance above 10 is obtained with S/B ratios close to 3 after double jet tagging for 3 years at low luminosity. Even by increasing the backgrounds by a factor of 3 and taking into account the efficiencies obtained with full simulations, the significance is above 6 after 3 years at low luminosity.

After one year at high luminosity, the significance is close to 12 and the signal to background ratio around 1. By requiring higher tag jet energies, the results could be substantially improved.

Based on those results, we would be tempted to conclude that the discovery of a heavy Higgs would be assured at the LHC. However, as can be seen in figure 11, the shape of the reconstructed background is very similar to that of the reconstructed Higgs mass. The high p_T cuts effectively raise the reconstructed mass of the background. Some caution must be exercised in the interpretation of the statistical significance since our knowledge of the actual background cross section is rather limited. Also the kinematics of the background could be quite different than what is predicted by the models used here, especially in the far tails of the distribution.

It is important to distinguish two kinds of uncertainties in the present

Cuts	H $\rightarrow$ WW $\rightarrow l\nu jj$	H $\rightarrow$ ZZ $\rightarrow lljj$
Cuts Leptons	$p_T^l,\ p_T^\nu > 50$ GeV $p_T^{W\rightarrow l\nu} > 150$ GeV	$p_T^{l_1},\ p_T^{l_2} > 50$ GeV $p_T^{Z\rightarrow ll} > 150$ GeV
Cuts Jets	$p_T^{W\rightarrow jj} > 150$ GeV 2 jets de $p_T^j > 50$ GeV with ΔR=0.2	$p_T^{Z\rightarrow jj} > 150$ GeV idem
Mass cut	$m_W \pm 10$ GeV	$m_Z \pm 15$ GeV

Table 14: Loose p_T cuts for H $\rightarrow$ WW $\rightarrow l\nu jj$ et H $\rightarrow$ ZZ $\rightarrow lljj$.

discussion. The first has to do with our ignorance of the production cross section of the background, particularly W+jets. However, it was shown that even by tripling the number of background events, the signal could still be extracted. In any case, once the experiment is taking data, this cross section will be known with much more accuracy. The second type of uncertainty has to do with the expected number of events after the imposition of all cuts for a given cross section. Taking into account the signal to background ratios obtained here, our modelization of the background kinematics would have to be extremely bad for the signal not to be visible. One must note that the W+jets kinematics can be studied using the Z+jets data set, which would contain very few signal events.

To make the above conclusions more robust, an independent evaluation of the reconstructed background mass shape should be performed. Ideally, one would evaluate the background on each side of the Higgs mass peak. However, for the heavy Higgs, the mass peak is very large and it would be very difficult to measure the side-bands around the mass peak. The strategy will consist of lowering the p_T cuts so that the reconstructed mass of the background does not peak close to the signal.

	Higgs	$t\bar{t}$ $p_T >$ 120 GeV	W+jets $p_T >$ 100 GeV	WW $p_T >$ 50 GeV
# Events	5000	2 400 000	5 200 000	255000
Central cuts low p_T et $m_W \pm$ 10 GeV	45.7%	1.7%	.2%	.8%
# Events	2285	40946	7855	2067
Veto 20 GeV	64.5%	7.4%	44.0%	56.4%
Veto 30 GeV	68.6%	14.7%	54.0%	65.6%
# Events Veto 20 GeV	1473	3046	3447	1167
Forward jet tag $>$ 300 GeV	50.7%	3.0%	0.9%	0.3%
# Events	747	90	31	3

Table 15: Low p_T cut efficiencies for the signal (M_H=1 TeV) and backgrounds.

8 H $\rightarrow$ WW $\rightarrow l\nu jj$ Results for Loose p_T cuts.

The "loose" central p_T cuts are given in table 14. Figure 12a shows the shape of the resulting reconstructed mass. The distributions are obtained with the two main backgrounds: W+jets and $t\bar{t}$. The lower cut-off of the recontructed mass for the background is no longer close to 700 GeV but rather around 400 GeV. Figure 12b shows the background after the imposition of a 30 GeV jet veto and double jet tagging with a threshold of 400 GeV. Figure 12c shows the reconstructed mass distribution for the background and signal. A clear peak can be observed. Figures 13 and 14 give the evolution of the background and signal shape for different tagged jet energy thresholds for Higgs masses of 1 TeV and 800 GeV, respectively. The jet veto threshold used is 30 GeV.

To evaluate the statistical significance of the signal peak relative to the background or to determine the probability that the shape of the reconstructed mass distribution is compatible with the background shape alone, the Kolmogorov-Smirnov test will be used.

8.1 Results with the Kolmogorov-Smirnov Test

The top-left plot of figure 15 shows the shape of the reconstructed mass and main backgrounds before jet tagging. The number of events corresponds to 3 years at low luminosity. The top-right plot shows the reconstructed mass distribution without the signal. The Kolmogorov-Smirnov (KS) probability that those two distributions are compatible with each other is 83%. The other plots on the figure show the evolution of the mass shape of the backgrounds for different energy cuts on the forward jets. In all those plots, the KS probability is always higher than 20%. Therefore, jet tagging does not change in a significant way the shape of the reconstructed mass for the main backgrounds.

This last characteristic will be exploited in the current analysis. It allows the comparison of signal plus background mass distributions with jet tagging with the shape of the signal plus background without jet tagging. This last distribution will be referred to as our reference distribution.

The top-left plot of figure 16 shows the reconstructed mass of the signal, normalized to 3 years at low luminosity. Although normalized, the number

of events used in the signal sample is much larger than the actual number of events one expects. Therefore, the fluctuations are not realistic. In the case of the backgrounds, the reverse is true. To be conservative, realistic fluctuations will only be implemented for the signal. This is shown in the top-right plot of figure 16 where the efficiencies obtained with full simulation have also been taken into account. The center-left plot shows the reconstructed mass distribution for a jet veto of 30 GeV and an energy cut of 400 GeV on the forward jets. For the center-right plot, the number of W+jets events was doubled and the $t\bar{t}$ background was increased by 50%. The two bottom plots show the equivalent distributions when the jet veto threshold is 20 GeV. The K-S probabilities are lower than 10^{-12} and 10^{-8} for the left and right plots, respectively.

The corresponding probabilities are all lower in the case of the 800 GeV Higgs.

9 Mass Distribution Fits

Should a mass peak be observed, the next step would be to determine the properties of this resonance. To do so, the position, width, and height of the peak would have to be determined.

To make an approximative evaluation of how well these quantities could be determined, the following fit to the mass peak was performed:

- An exponential is used to fit the background.
- A Breit-Wigner distribution whose width is proportionnal to $(M_H)^3$ was used for the signal and whose amplitude decreases exponentially :

$$f(x) = \frac{a \cdot e^{-k \cdot x} \cdot \frac{b \cdot (\frac{x}{1000})^3}{2\pi}}{\frac{(b \cdot (\frac{x}{1000})^3)^2}{4} + (x - c)^2} \qquad (1)$$

The constant k was fixed for all the fits. Figure 17 shows on the left side, the fits done on the reconstructed mass distribution for M_H=800 and 1000 GeV[7]. For these fits, only parameters a and c were allowed to change and

[7]Also shown are fits for M_H=600 GeV. More details for this mass range can be found in [10].

parameter b was fixed at 500 GeV. As can be seen from these fits the signal shape is well reproduced by the analytic form. On the right of the figure the free parameters are the central value and height of the Breit-Wigner and the height of the exponential tail describing the background. The error obtained on the central value of the mass peak is less than 5%. The error on the height is about 20%.

In figure 18, the central value of mass peak is fixed (parameter c) while the width, which depends on parameter b, is left free. The error on this parameter is about 30% .

10 H $\rightarrow$ ZZ $\rightarrow$ $lljj$ Results

The production rate for the H $\rightarrow$ ZZ $\rightarrow$ $lljj$ signal is about 6 times lower than the H $\rightarrow$ WW $\rightarrow$ $l\nu jj$ signal. For this reason, this channel is not able to compete with H $\rightarrow$ WW $\rightarrow$ $l\nu jj$ despite the fact that $t\bar{t}$ is not a significant background. However, the study of H $\rightarrow$ ZZ $\rightarrow$ $lljj$ could be used to confirm the presence of a Higgs signal with different backgrounds. The ZZ and WZ backgrounds are about 10% of the Z+jets background before jet tagging and are negligible after jet tagging.

Using the "high" p_T cuts that were shown in table 2, a statistical significance of less than 3 is obtained for $m_H \geq 800$ GeV after 3 years at low luminosity. This search must therefore be made in the high luminosity environment.

Table 16 gives values of $\frac{S}{\sqrt{B}}$ and S/B ratios for one year at high luminosity using high p_T cuts for m_H=1 TeV and m_H=800 GeV. For each Higgs mass, the last row takes into account the efficiencies obtained with full simulation and with pile-up noise. The number of fake jets (fj) is indicated in parentheses.

Based on the results presented above and more detailed studies done in [10], we estimate that a clear observation of a signal would require 2 to 3 years at high luminosity.

	Higgs	Z+jets p_T >100 GeV		
# Events	5000	5 000 000	$\frac{S}{\sqrt{B}}$	$\frac{S}{B}$
1 year high lumi.	260	4 800 000		
M_H = 1000 GeV				
(Forward jets 600 GeV)	9.2	2	6.5	4.6
(Forward jets 300 GeV)	17.3	8	6.1	2.2
with efficiencies	14.7	6.4 + (12 fj)	3.4	0.8
M_H = 800 GeV				
(Forward jets 600 GeV)	9.4	2	6.6	4.7
(Forward jets 300 GeV)	19.2	8	6.8	2.4
with efficiencies	16.3	6.4 +(12 fj)	3.8	0.9

Table 16: Statistical significance and signal to noise ratios for $M_H \geq 800$ GeV. For each Higgs mass, the last row takes into account the efficiencies obtained with full simulation and with pile-up noise.

11 Conclusions

Full simulations of the heavy Higgs signal and backgrounds were performed and the efficiencies for reconstructing the W $\rightarrow$ jet-jet decay, for vetoing jets in the central region ($|\eta| < 2.0$) and tagging jets in the forward region ($2.0 < |\eta| < 4.9$) have been evaluated and compared to ATLFAST. In general, very good agreement between ATLFAST and DICE was observed for most of the quantities that were measured. Some discrepancies were observed however, particularily in the reconstruction of the forward jet at η >4.0.

Using the efficiencies mentioned above, the discovery potential was evaluated in the second part of the note. We conclude that a heavy Higgs could be found with ATLAS after 3 years of low luminosity running (3×10^4 pb^{-1}) of the LHC.

Acknowledgments

We would like to thank:

- Luc Poggioli and Daniel Froidevaux for very helpful discussions.
- Peter Loch for helpful discussions on jet reconstruction in the forward calorimeter and for the use of his simulation program.

References

[1] J. Erler and P. Langacker, Proceedings of the 5th International WEIN Symposium: A Conference on Physics beyond the Standard Model (WEIN 98), Santa Fe, NM, 1998. (hep-ph/9809352)

[2] M.S. Chanowitz, Phys. Rev. Lett. 80 (1998) 2521 (hep-ph/9710308); and hep-ph/9807452

[3] see, e.g., M. Peskin, Proc. of the 1996 European School of High-energy Physics,Carry-le-Rouet, France (hep-ph/9705479)

[4] H. Ruiz and M. Bosman, ATLAS phys. note in preparation and H. Ruiz, tesina, Univ. of Barcelona (1998).

[5] V. Cavasinni, D. Costanzo, S. Lami and F Spanò, ATLAS-PHYS-127

[6] Zmushko, Poggioli and Froidevaux, ATLAS Internal Note PHYS-NO-103 (1997).

[7] The ATLAS Collaboration, ATLAS Technical Proposal, CERN/LHCC/94-43 LHCC/P2,(1994).

[8] Zmushko, Poggioli and Froidevaux, ATLAS Internal Note PHYS-NO-008 (1992).

[9] D.C. O'Neil, Master's Thesis, University of Alberta (1996).

[10] P. Savard, Ph.D. Thesis, Université de Montréal (1998).

[11] T. Sjostrand, PYTHIA 5.7 and JETSET 7.4 Manual, CERN-TH-7112/93

[12] E. Richter-Was et al., ATLAS Internal Note PHYS-NO-79 (1996).

[13] R. Brun and F. Carninati, GEANT Detector Description and Simulation Tool, CERN Programming Library Long Writeup W5013 (1993).

[14] R.A. Davis and P. Savard, ATLAS Internal Note CAL-NO-84 (1996).

[15] R.A. Davis, D O'Neil, and P. Savard, ATLAS Internal Note CAL-NO-89 (1996).

[16] ATLAS Collaboration, Calorimeter Performance Technical Design Report, CERN/LHCC/96-40.

[17] M. Cobal, D. Costanzo and S. Lami, Internal Note PHYS-NO-84 (1996).

[18] P. Savard, ATLAS Internal Note CAL-NO-92 (1997).

[19] R.D. Field, P.A. Griffin Phys.Rev.D48, 3167-3173, (1993).

[20] H. Kuijf et *al.*, proc. of the Large Hadron Collider Workshop (aachen, 1990), vol. II, p. 91, eds: G. Jarlskog and D. Rein;
M. Cobal, D. Costanzo and S. Lami, ATLAS note INDET-026 (1993) and references therein

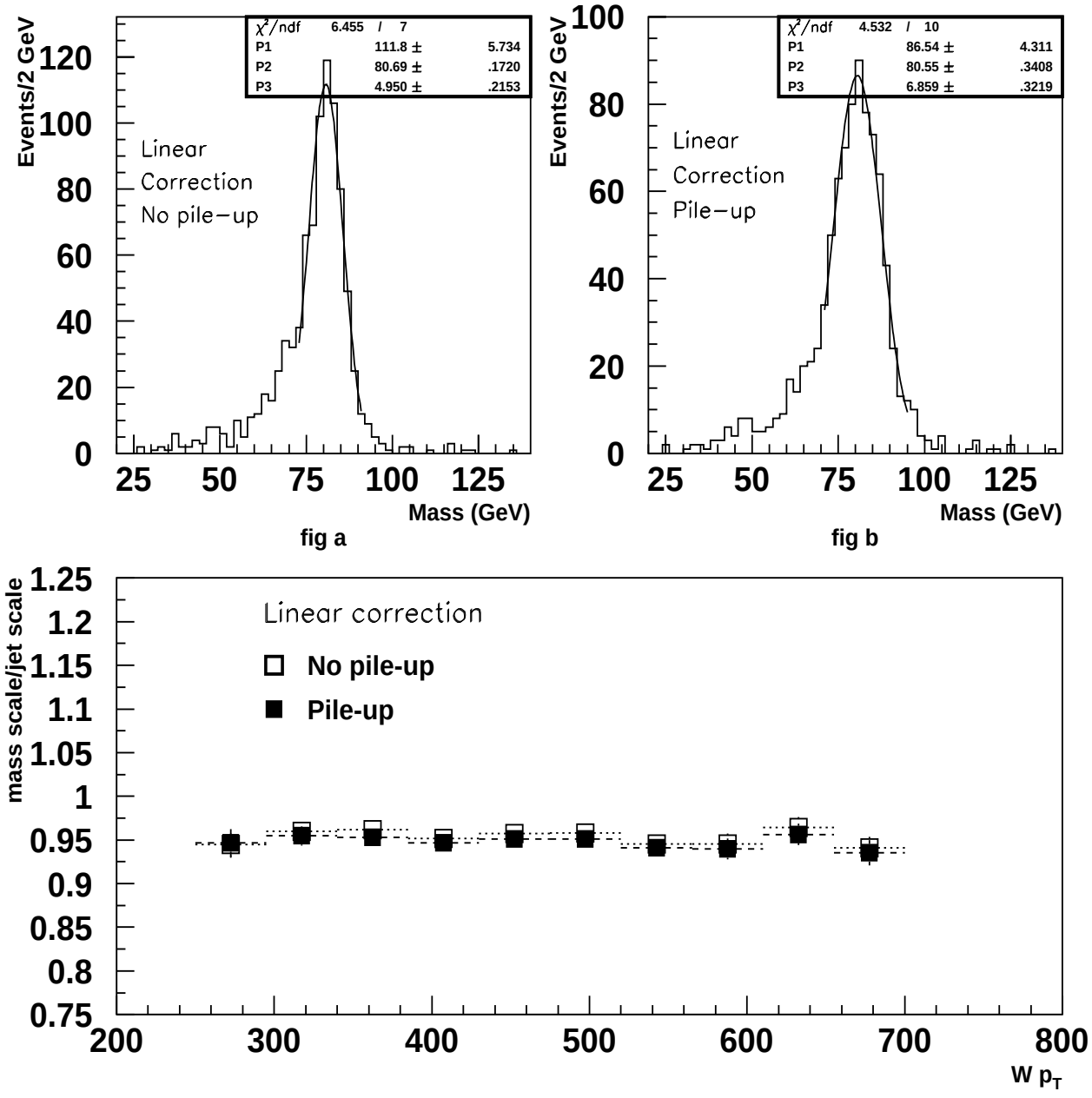

Figure 2: Upper plot: the reconstructed W mass after applying a linear correction which is a function of the W p_T. Lower plot: The ratio if the mass scale over the energy scale after aplying the correction.

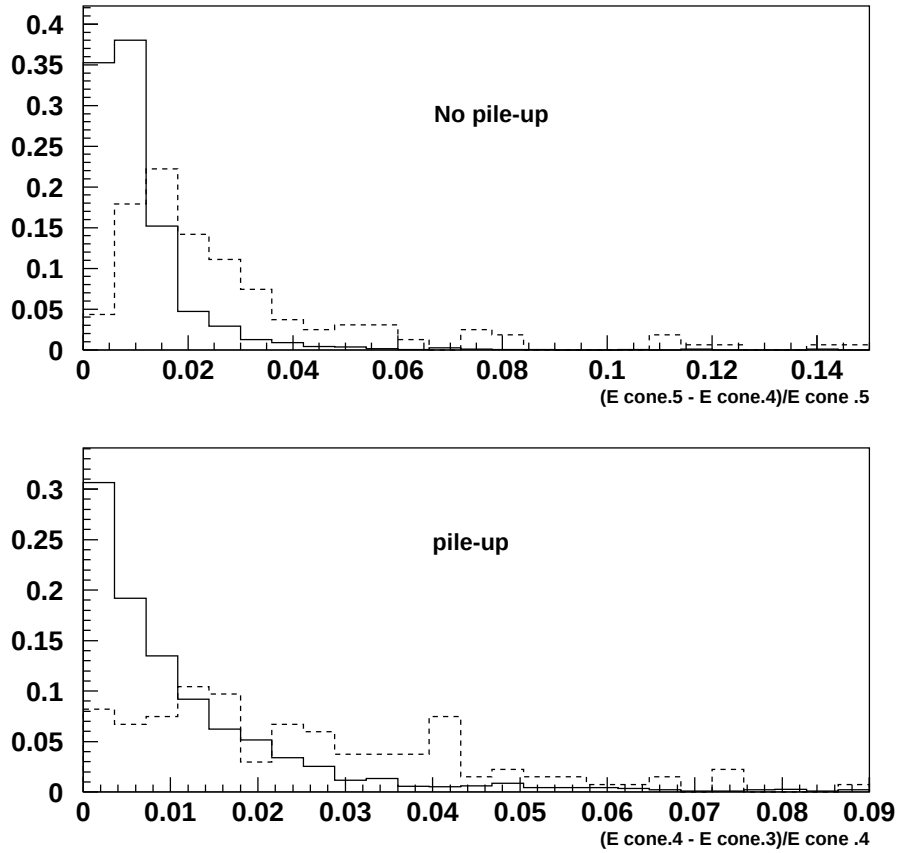

Figure 3: The jet profile (see text) variable used to descriminate between the signal (full line) and W+jets (dashed line).

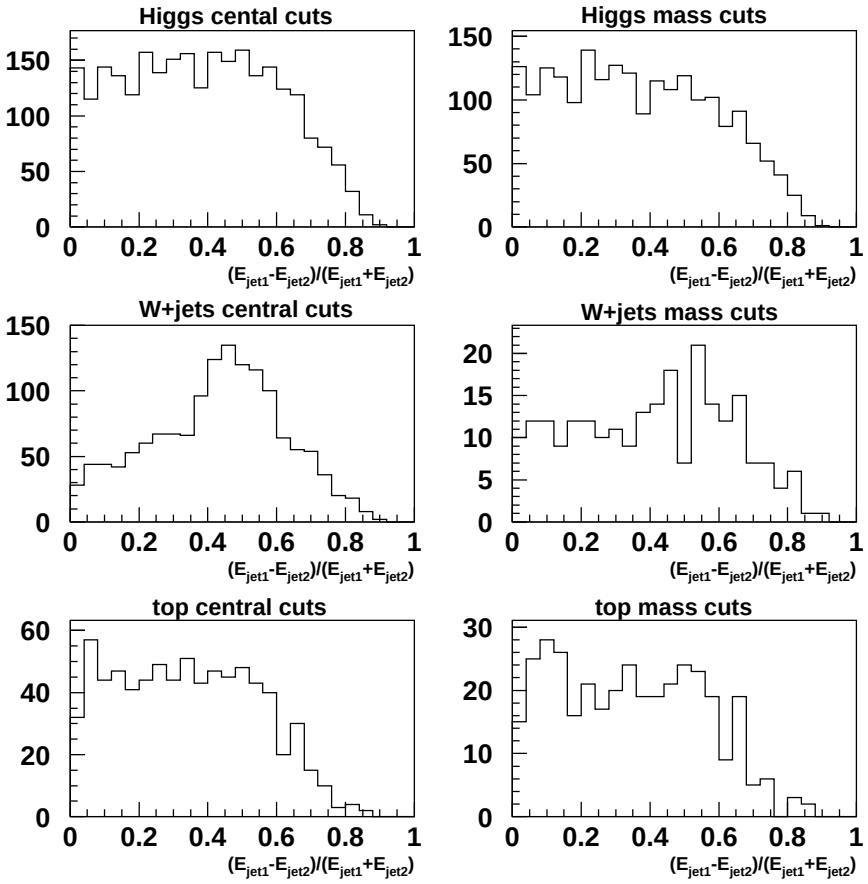

Figure 4: The energy asymmetry of the W jet candidates. The plots on the left show the asymmetries obtained with the central cuts only. The plots on the right show the asymmteries obtained after a cut on the W mass.

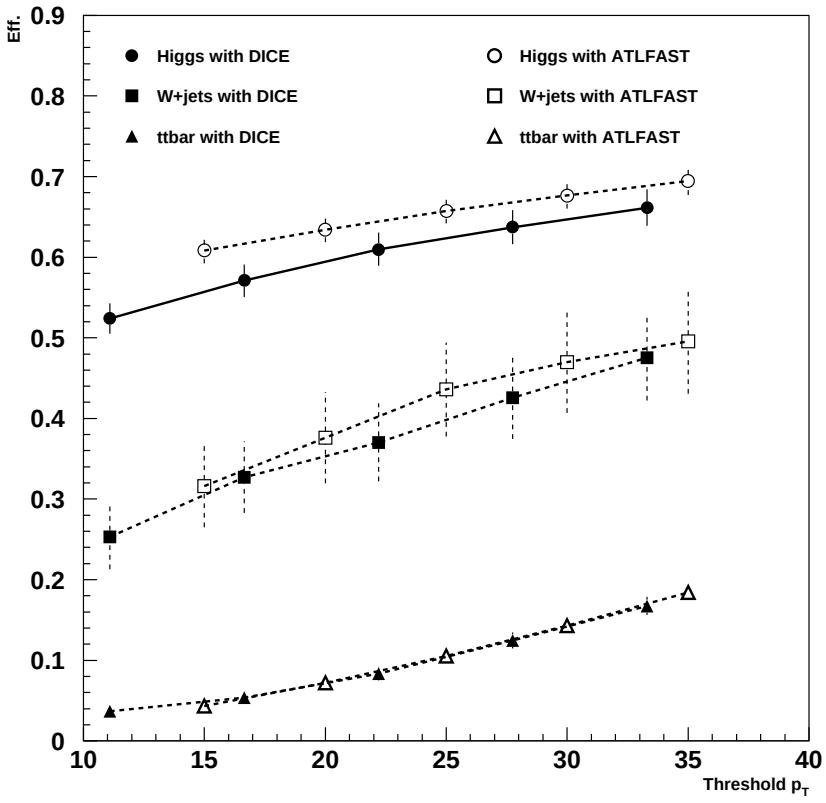

Figure 5: Comparison of the jet veto efficiency in the central region obtained with ATLFAST and DICE.

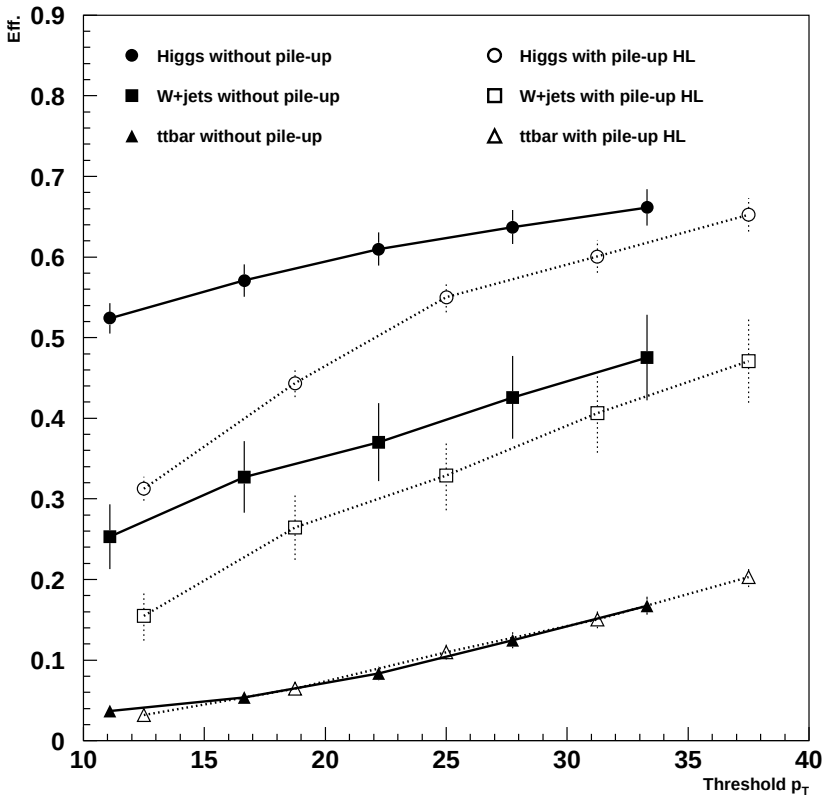

Figure 6: Comparison of the jet veto efficiency with and without high luminosity pile-up noise.

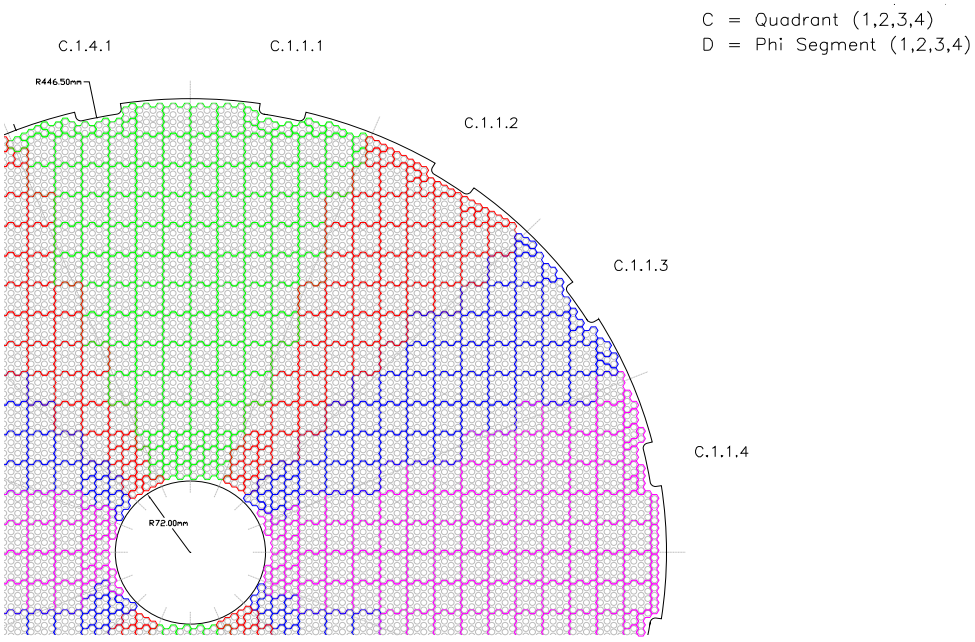

Figure 7: Tile readout scheme in x and y for the forward calorimeter

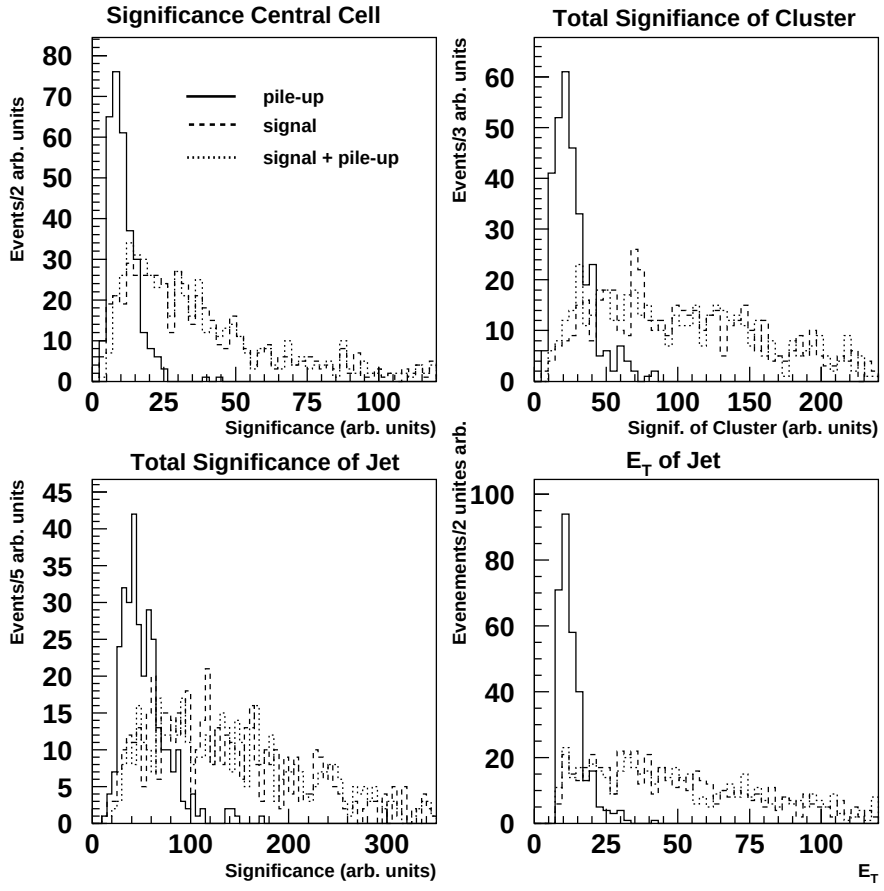

Figure 8: The top left plot shows the significance of the jet seed cell in the FCAL region. The top right plot gives the total significance in a ΔR=0.2 cone (the sum is linear) around the seed sell. A cone of ΔR=0.4 is used in the bottom left plot. The transverse energy of the jet is shown in the bottom right plot.

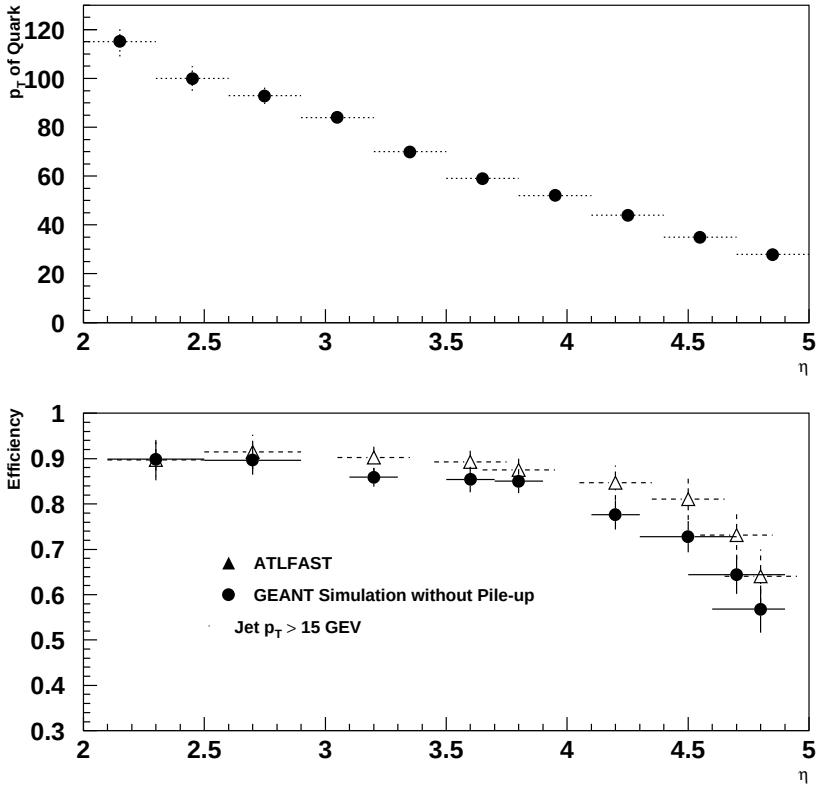

Figure 9: The bottom plot shows the average transverse energy of forward quarks as a function of η. The bottom plot gives the jet tagging efficiency for ATLFAST and the full GEANT simulation.

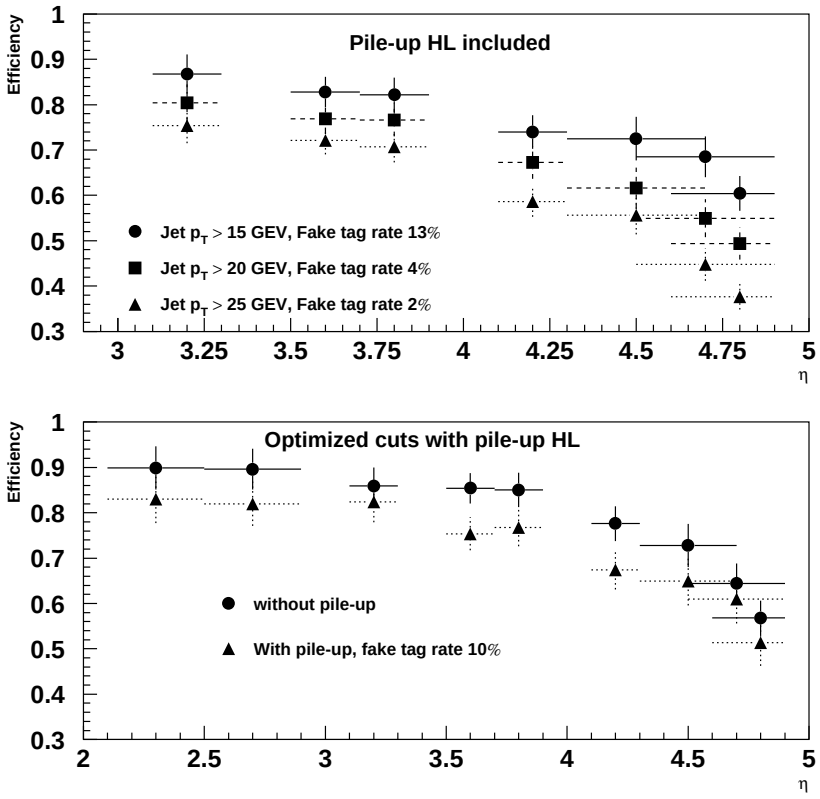

Figure 10: Upper plot: jet tagging efficiencies with pile-up noise for different jet p_T cuts. Bottom plot: Optimized efficiency for a fake tag rate of 10%. With an energy cut of 300 GeV, the fake tag rate drops from 10% to 3%.

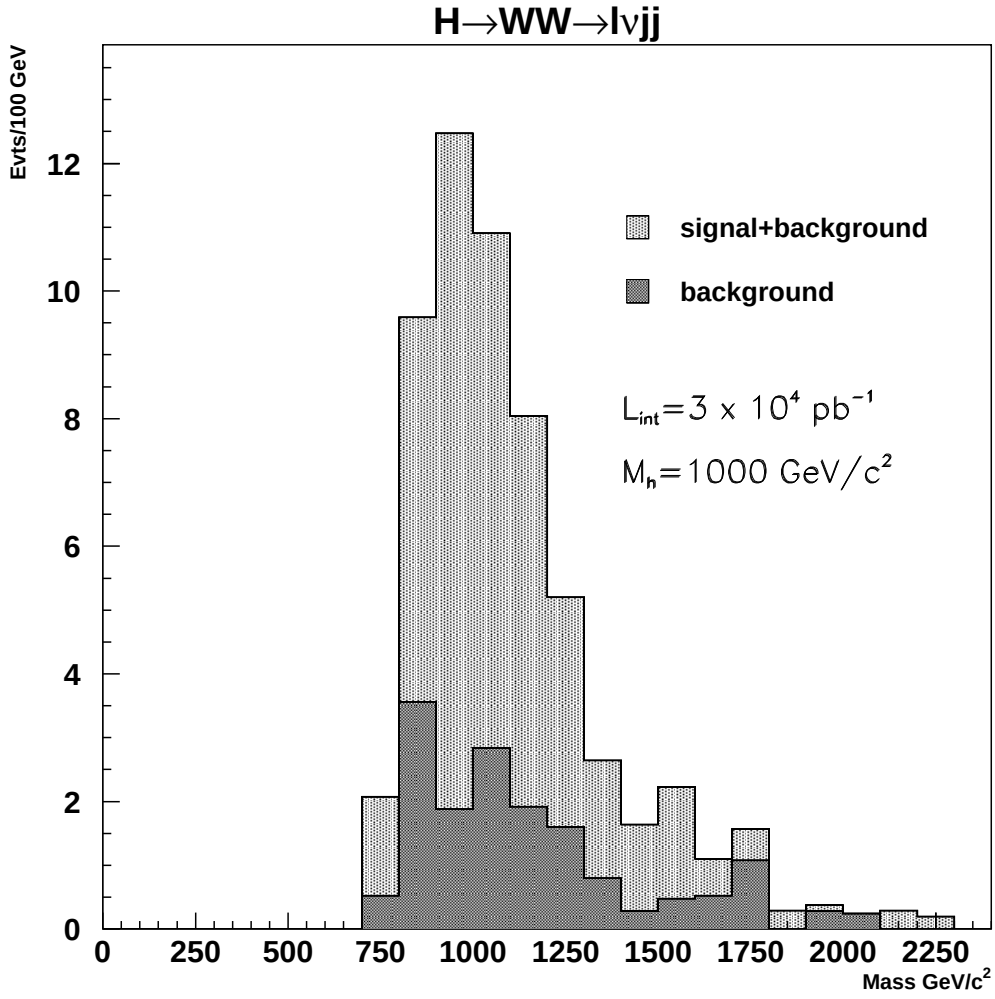

Figure 11: The reconstructed Higgs mass for M_H=1 TeV. The tagged jet energy cut was 100 GeV.

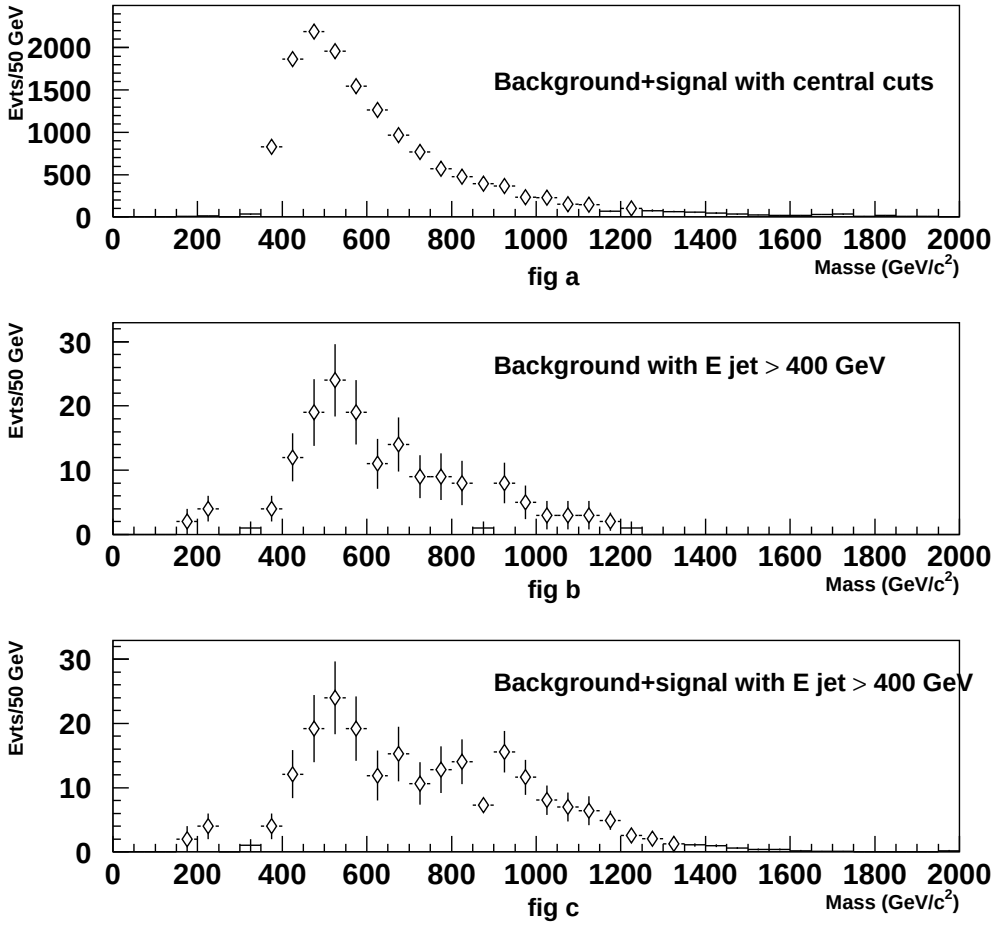

Figure 12: Shape of the reconstructed mass distribution after the imposition of loose central p_T cuts. The Higgs mass is 1 TeV.

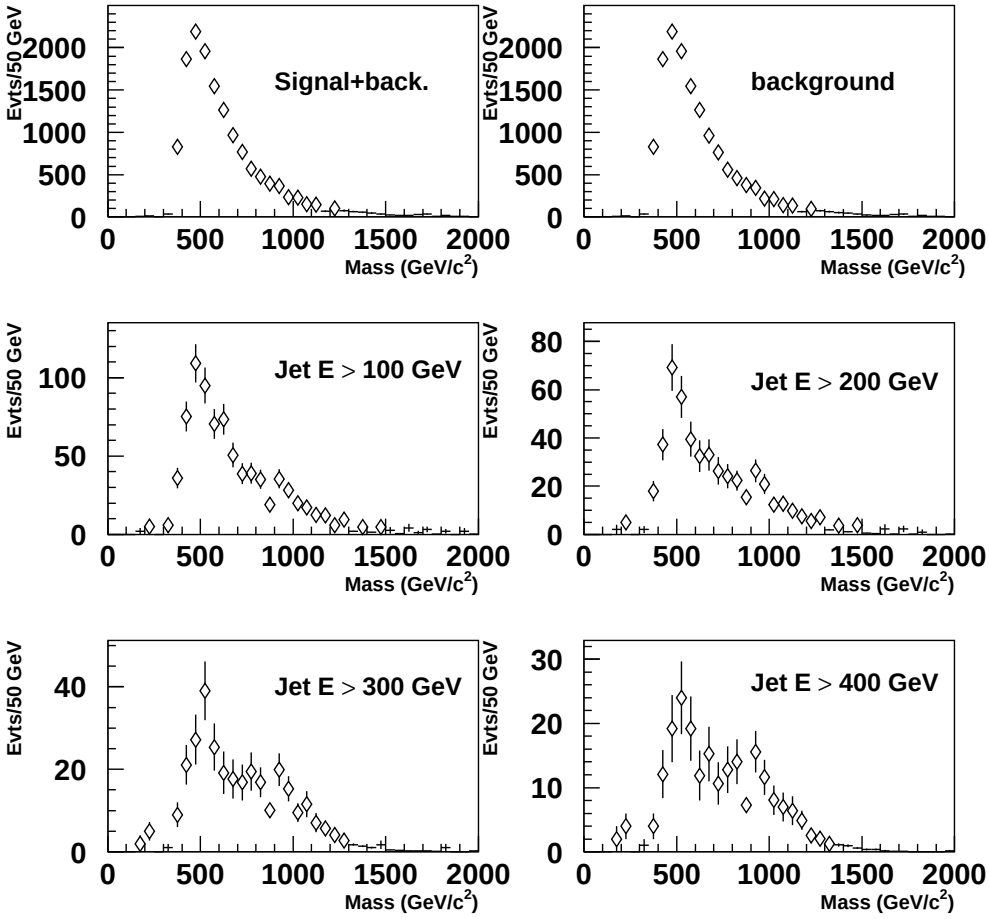

Figure 13: Shape of the reconstructed mass with the central loose p_T cuts for different thresholds on the jet tag energy. The Higgs mass is 1 TeV.

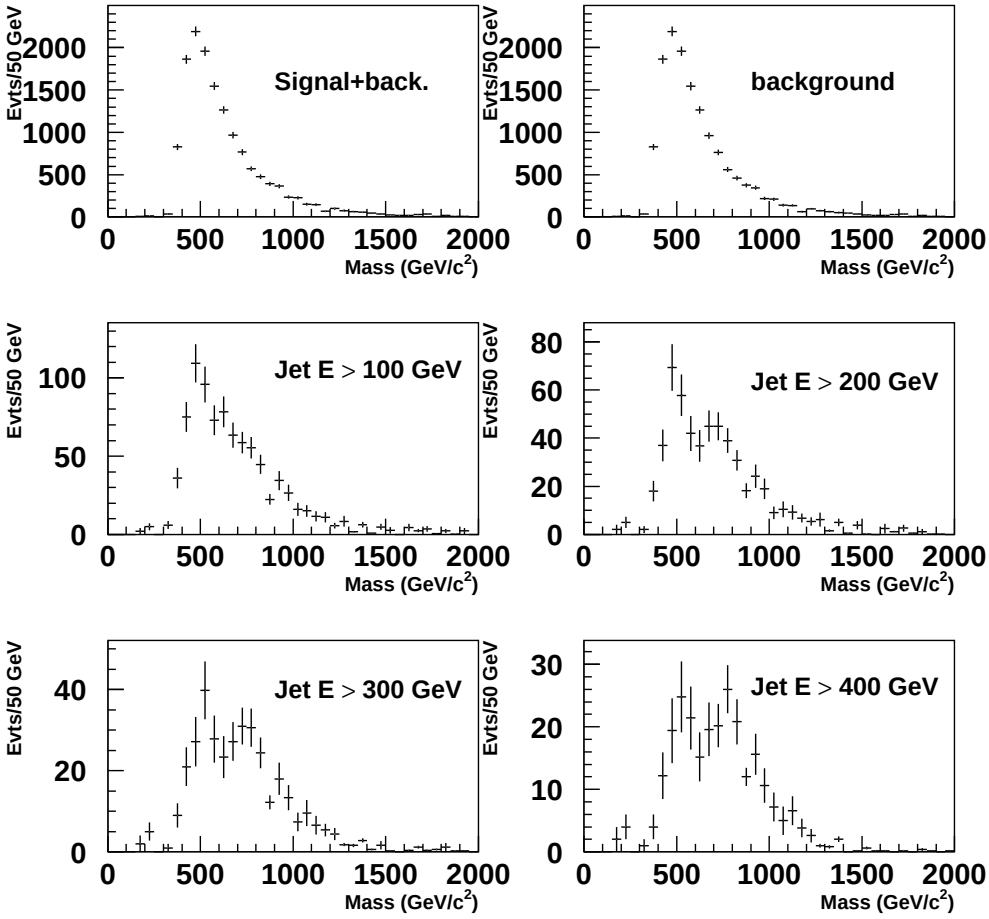

Figure 14: Shape of the reconstructed mass with the central loose p_T cuts for different thresholds on the jet tag energy. The Higgs mass is 800 GeV.

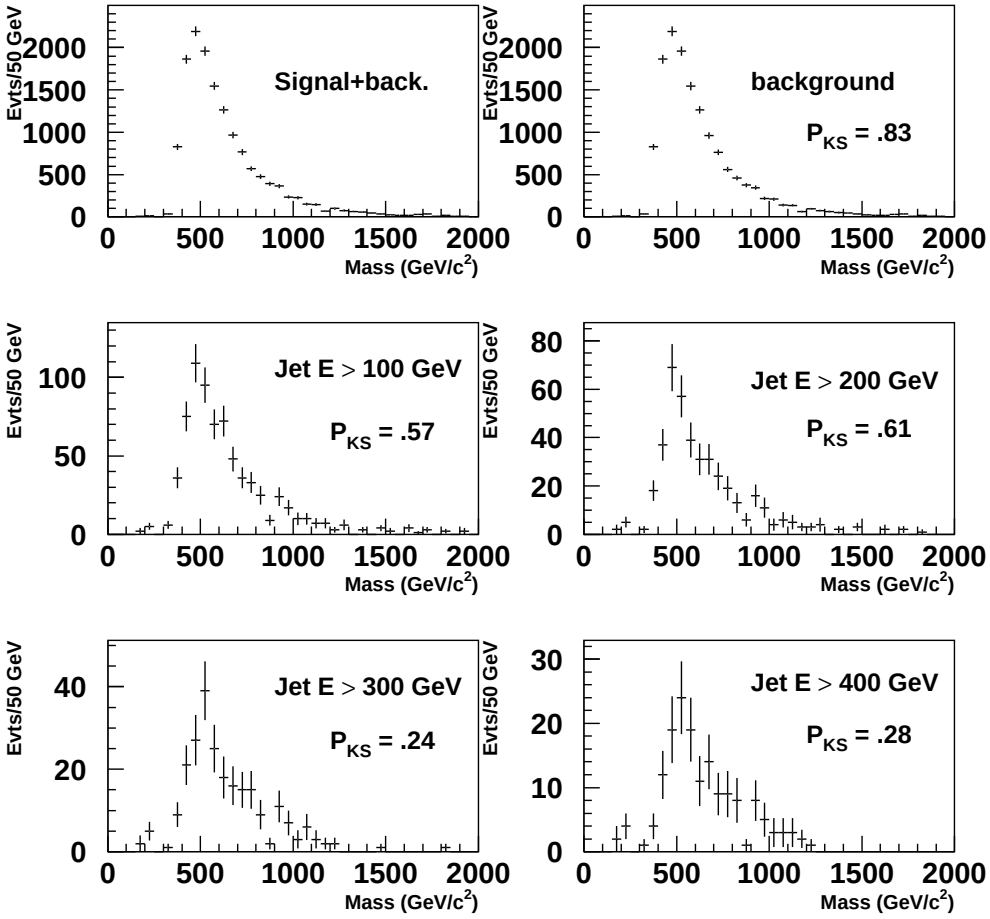

Figure 15: Shape of the reconstructed background distribution after applying the "loose" p_T cuts for different energy cuts on the forward jets. P_{KS} refers to the Kolmogorov-Smirnov probability (see text). The Higgs mass is 1 TeV.

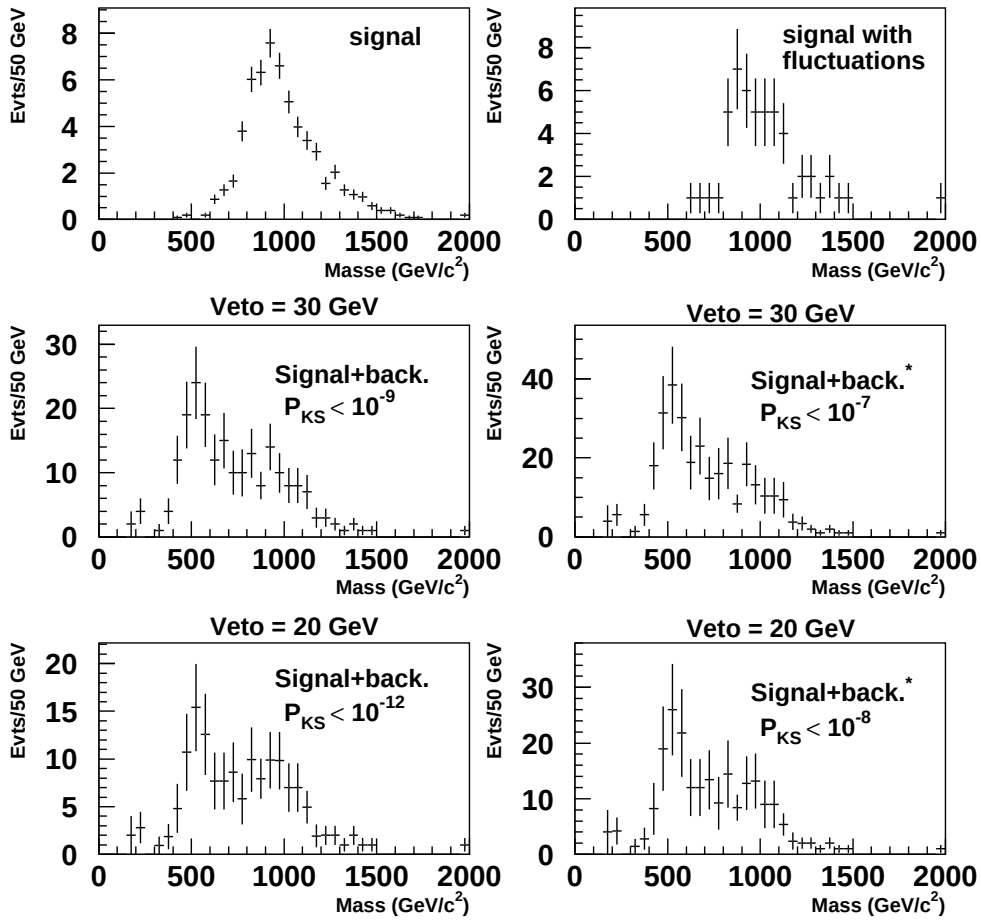

Figure 16: Shape of the reconstructed background distribution after applying the "loose" p_T cuts for different energy cuts on the forward jets. P_{KS} refers to the Kolmogorov-Smirnov probability (see text). The Higgs mass is 1 TeV.

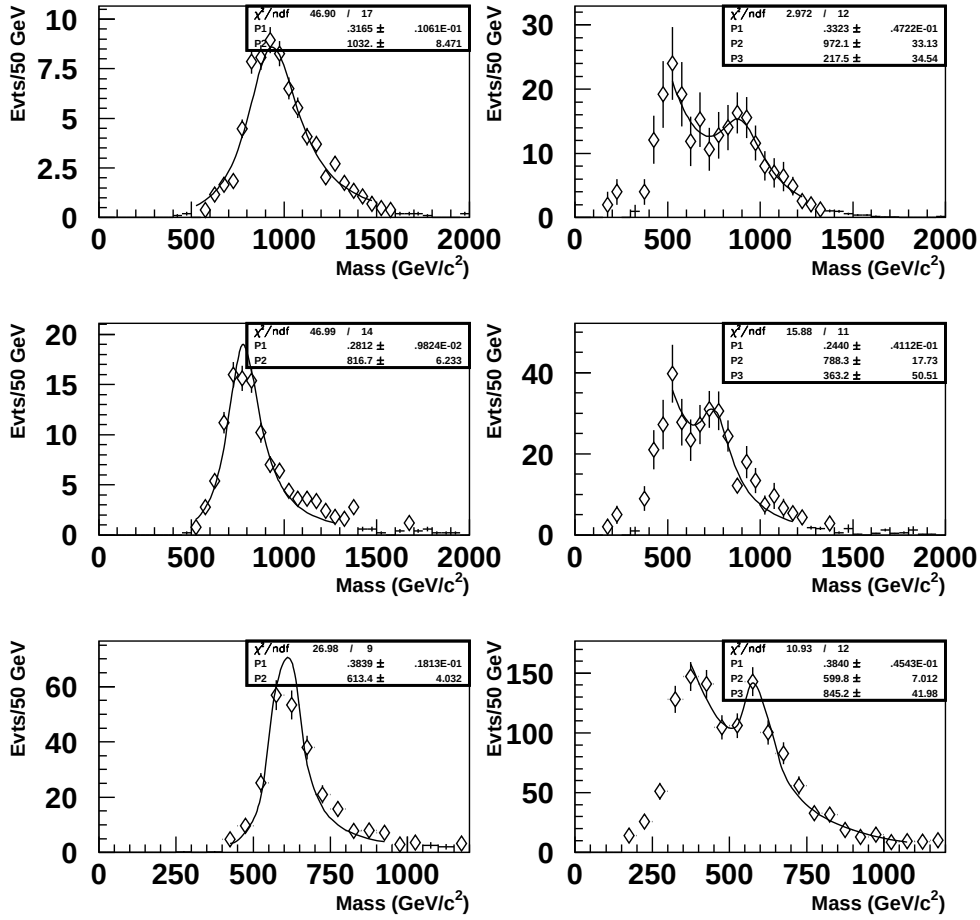

Figure 17: Reconstructed mass distribution fitted for the signal (left) and for the signal and backgrounds (right). The fitted quantities are the height of the signal and background distributions and the central value of the mass peak.

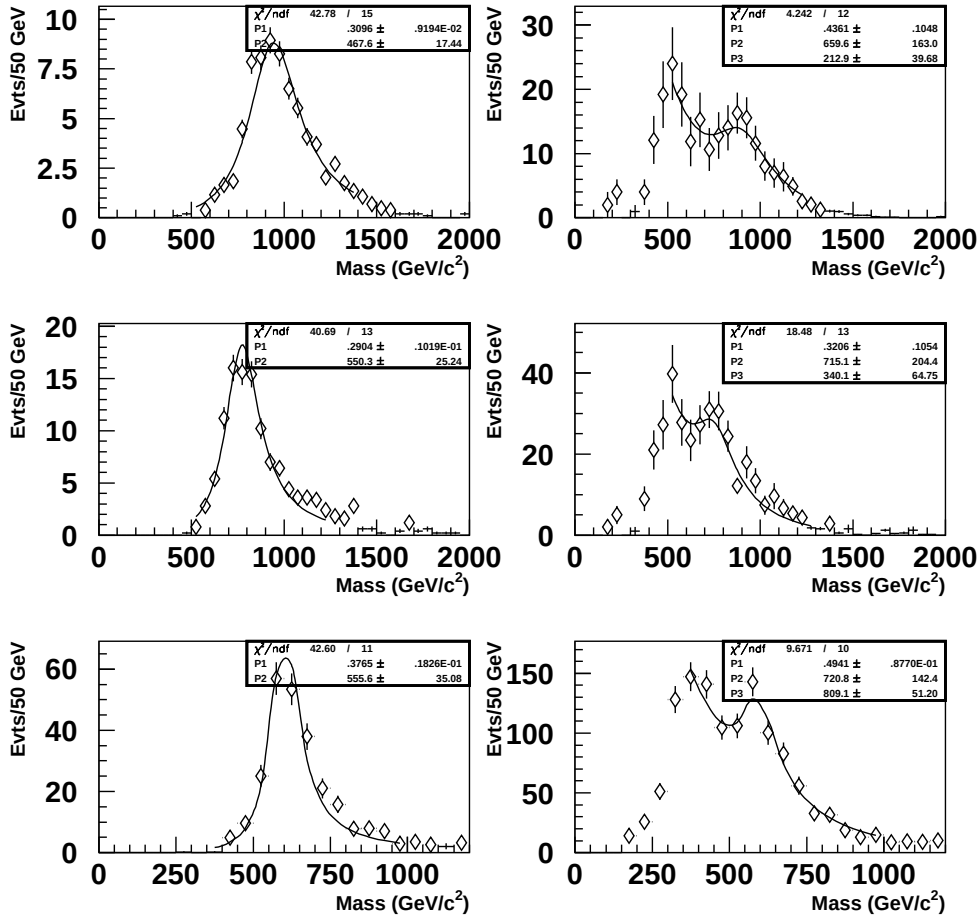

Figure 18: Reconstructed mass distribution fitted for the signal (left) and for the backgrounds (right). The fitted quantities are the height of the signal and background distributions and parameter b, which depends on the signal width.